J. Astrophys. Astr. (2006) **27,** 267–276

Extremely Energetic 4B/X17.2 Flare and Associated Phenomena

Wahab Uddin*, Ramesh Chandra & Syed Salman Ali
Aryabhatta Research Institute of Observational Sciences (ARIES), Manora Peak, Nainital 263 129, India.
**e-mail: wahab@upso.ernet.in*

Abstract. We observed 4B/X17.2 flare in Hα from super-active region NOAA 10486 at ARIES, Nainital. This is one of the largest flares of current solar cycle 23, which occurred near the Sun's center and produced extremely energetic emission almost at all wavelengths from γ-ray to radio-waves. The flare is associated with a bright/fast full-halo earth directed CME, strong type II, type III and type IV radio bursts, an intense proton event and GLE. This flare is well observed by SOHO, RHESSI and TRACE. Our Hα observations show the stretching/de-twisting and eruption of helically twisted S shaped (sigmoid) filament in the south–west direction of the active region with bright shock front followed by rapid increase in intensity and area of the gigantic flare. The flare shows almost similar evolution in Hα, EUV and UV. We measure the speed of Hα ribbon separation and the mean value is $\sim 70\,\mathrm{km\ s^{-1}}$. This is used together with photospheric magnetic field to infer a magnetic reconnection rate at three HXR sources at the flare maximum. In this paper, we also discuss the energetics of active region filament, flare and associated CME.

Key words. Sun: Flares, coronal mass ejections, reconnection.

1. Introduction

The period of late October to early November 2003 was characterized as the highest levels of solar activity to date when the solar cycle 23 was well into the decline phase. The extreme level activity began with the appearance of three most complex superactive regions NOAA 10484, 10486 and 10488. These active regions produced a series of powerful flares, large coronal mass ejections (CMEs) as well as strong space weather disturbance. NOAA 10486 grew to be the largest sunspot group of the current solar cycle and it produced many spectacular solar events, including the most energetic flares 4B/X17.2 on 28 October, the 2B/X10 on 29 October and the 3B/X28 on 4 November 2003 and their associated fast halo CMEs, different types of extraordinary radio bursts. Many authors studied these flares and associated phenomena at different wavelengths (Luthi *et al.* 2004; Pick *et al.* 2005; Klassen *et al.* 2005; Donea and Lindsey 2005; Gopalswamy *et al.* 2005; Grechnev *et al.* 2005).

In this paper, we present the preliminary analysis of X17.2 flare, observed on 28 October 2003. We examined the Hα morphology of the flare and compared it with TRACE EUV/UV, RHESSI HXR and MDI magnetogram data. We also studied the energetics of sigmoid filaments, flare and associated CME.

2. Observations

During the decay phase of solar cycle 23, on 28 October 2003 we observed a long duration super flare 4B/X17.2 in Hα from NOAA 10486 at the location S16 E08, at ARIES, Manora Peak, Nainital, India. The observations were using 15 cm, f/15 Coudé Solar Tower Telescope equipped with Bernhard Halle Hα filter and Wright Instrument CCD camera system (16 bit, 385 $\times$ 576 pixel, pixel size = 22 micron square). With the help of barlow lens the image has been magnified twice, so we get a resolution of $1''$ per pixel. The observed filtergrams were corrected using dark current and flat field images taken during the observations. All images were re-registered.

The flare has been simultaneously observed by RHESSI (Lin *et al.* 2002), TRACE (Handy *et al.* 1999), SOHO/LASCO (Brueckner *et al.* 1995) and SOHO/EIT (Delaboudiniere *et al.* 1995). This flare also produced several extremely strong radio bursts and it was well observed by the IZMIRAN, Potsdam Observatory and WAVES/WIND (Bougeret *et al.* 1995) spectrometers in a broad range of radio frequencies. To understand the magnetic topology of the active region we used SOHO/MDI (Scherrer *et al.* 1995) data.

3. Analysis and results

3.1 *Hα observations*

The evolution of the flare in Hα is shown in Fig. 1. The Hα movie shows large scale mass motions, darkening of filaments and brightening at many places in the active region before the flare onset. The first image taken well before flare at 01:28:36 UT shows the three highly twisted long sigmoid filaments (F1, F2 and F3), which started eruption before the onset of 4B/X17.2 class flare. The eruption of all three filaments continued during the flare.

The eruption of filament F1 plays an important role in the process of flare triggering and initiation of the CME and associated radio bursts. The filament F1 eruption shows detwisting in the clockwise direction. Before the major X17.2 flare an M8.4 class long duration flare peaked at 10:48 UT in the eastern side of the active region. This flare may be treated as the precursor phase for the main flare.

The 4B/X17.2 flare centered in the western part of the active region is the second largest flare event recorded during the solar cycle 23. The flare shows multi-ribbon structure in Hα. It consists of two main parallel ribbons along the sigmoid filament in opposite magnetic polarity regions (c.f. Fig. 2). These parallel Hα ribbons show the separation as shown by a typical two ribbon flare. We have estimated the ribbon separation speed and found it very high $\sim$ 70 km s^{-1}. Between 10:25 and 10:30 UT a remote ribbon appeared in south–west direction (filaments F1 and F3 eruption direction). The chronology of the Hα flare is given in Table 1.

To study the temporal evolution of the flare in Hα, we selected the three Hα kernels shown in Fig. 2. The temporal evolution of these flare kernels are shown in Fig. 3. Temporal evolution of the kernels show that all kernels evolve differently. Kernel 2 has more peak period in comparison to kernel K1 and K3. The time profiles show multiple peaks during its impulsive and maximum phase. This implies that multiple magnetic field reconnection occurs in the flaring processes successively. In millimeter

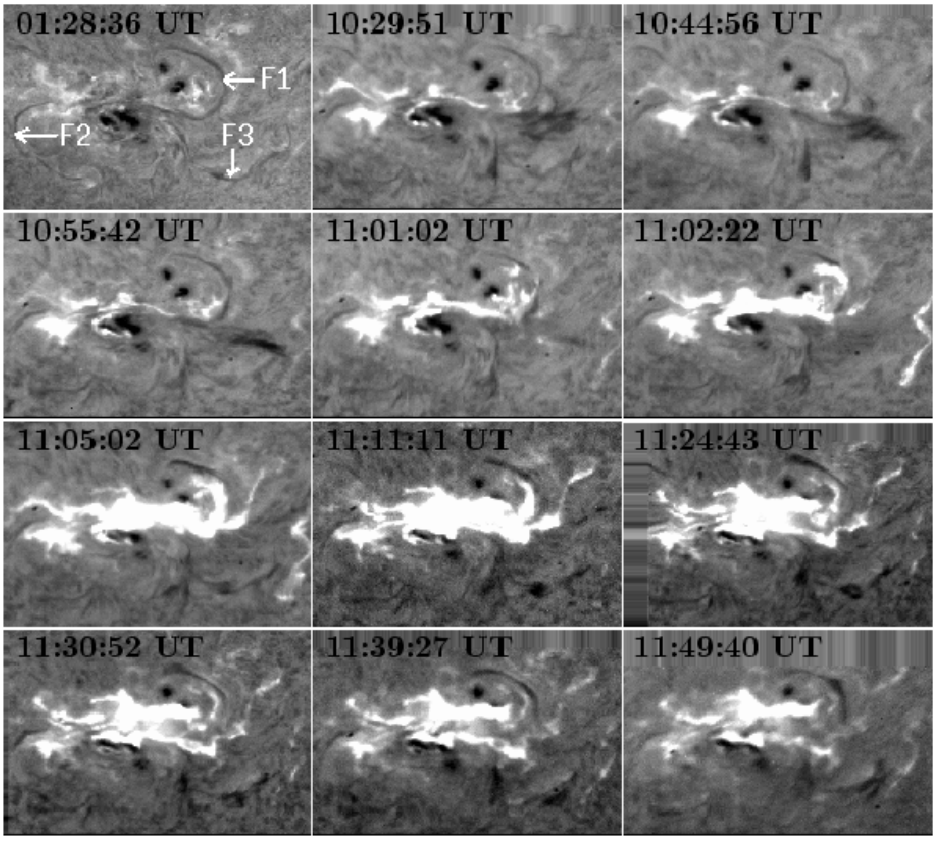

Figure 1. Evolution of historical 4B/X17.2 flare in Hα. North is up and west is to the right and the FOV is $505'' \times 384''$.

Table 1. Hα chronology of the flare.

Time (UT)	Important changes
06:00–07:00	Activation of filaments F1, F2 and F3 started
08:22	Bright knot like structure appeared near the main flare site
09:56	M1.3 flare started in the central part of the active region
10:09	M2.3 flare started in the eastern part of the active region
10:00–10:30	Sigmoid filament eruption started in S–W direction
10:25–10:30	Remote ribbon appeared in SW direction
10:48	M8.4 long duration flare peaked
10:58	Onset of massive X17.2 flare
11:02	Remote ribbon becomes very bright
11:00–11:11	Fast development of flare ribbons, fast ribbon separation starts and reached flare attains maximum
11:11	Flare maximum phase and the remote ribbon faded out
After 11:12	Bright Hα LOOP appeared joining kernel K1 and K3

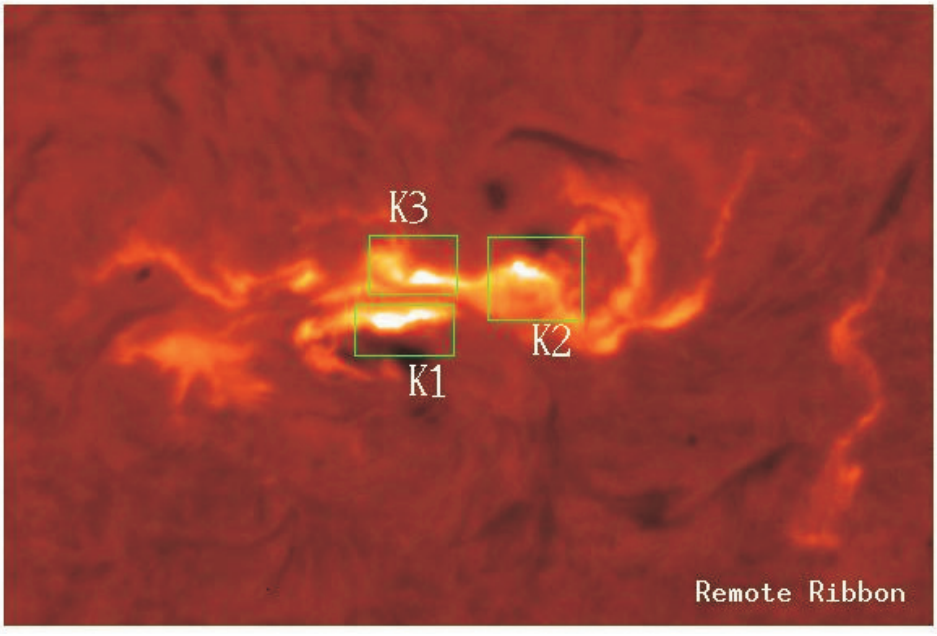

Figure 2. Hα image at flare maximum (11:04:36 UT). The different Hα kernels and remote brightening are shown in this figure. The FOV of the image is $574'' \times 384''$.

wavelength emission at 210 GHz shows two main features: a slowly varying component (11:02:30 to 11:2 UT) and a short lived component exhibiting three distinctive peaks between 11:03:45 and 11:06:10 UT (Luthi *et al.* 2004). A similar type of temporal evolution is also visible in Hα kernel K2, which indicates the acceleration of high energy electrons $\geq$ 0.5 MeV.

3.2 *Comparison of Hα data with UV, EUV and RHESSI data*

Figure 4 shows the start, maximum and decay phase of the 4B/X17.2 flare in Hα, UV (1600 Å) and EUV (195 Å) respectively. On comparison of these images we can say that the flare shows a similar type of morphological evolution in Hα, UV and EUV wavelengths. The flare ribbon's twisted structure which gets detwisted during flare evolution, is clearly visible in Hα and UV. Evolution of post flare loops joining the parallel ribbons show that the reconnection of higher and higher loops indicate prolonged energy release and relaxation of highly sheared magnetic field.

Figure 5 illustrates the plot of the magnetic field on Hα (upper left), MDI magnetogram overlaid by RHESSI HXR 100–200 keV sources location (marked by circle, upper right), TRACE 195 Å image overlaid by RHESSI 100–200 keV HXR contours (lower left) and the location of HXR sources at the selected times (lower right).

On comparison of the spatial location of Hα kernels and the location of HXR sources, it appears that the Hα kernels K1, K2 and K3 are associated with three HXR sources (c.f. Figs. 2 and 5). According to the study of Krucker & Hudson

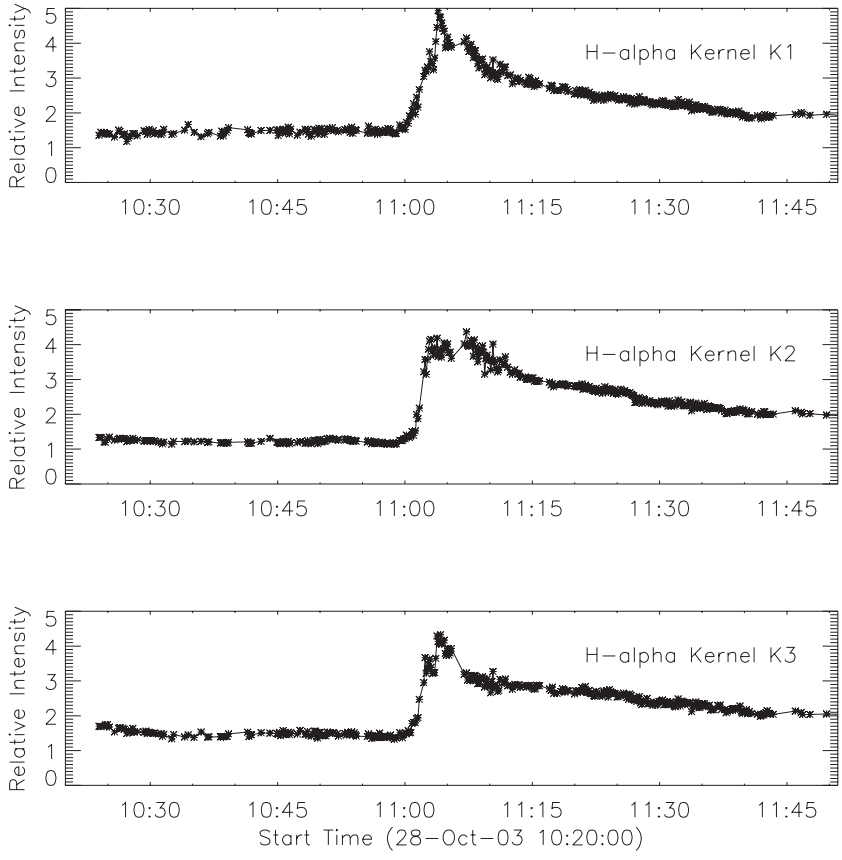

Figure 3. Temporal evolution of different flare kernels in Hα.

(2004) the two γ ray footpoints are embedded in the flare ribbons. Although close to the HXR centroid position, each γ ray footpoint is displaced to the east direction. Comparing the γ ray sources and Hα kernel locations it seems that the γ ray sources are close to the Hα kernels K1 and K2. Donea & Lindsey (2005) detected seismic wave emitted from this flare. The major acoustic sources are seen to coincide closely with HXR emissions from magnetic footpoints that terminate in the umbral or penumbral chromosphere of sunspots. We measure the strength of the magnetic field using MDI magnetogram at the Hα kernels K1, K2 and K3 associated with HXR sources and the measured values are 1000, -800 and -500 gauss respectively.

Figure 5 (lower right panel) shows the position of HXR sources at some selected times (taken from Sam Krucker web page). In general the motion of HXR sources during flare depends mainly on the magnetic field configuration. During a flare, magnetic reconnection provides powerful fluxes of energy along the reconnected field lines. As the flare progresses, the newly reconnected footpoints of the magnetic field lines move away from neutral line with a velocity proportional to reconnection rate. Similar to this explanation we noticed the motion in HXR sources away from the magnetic neutral line (c.f. Fig. 5).

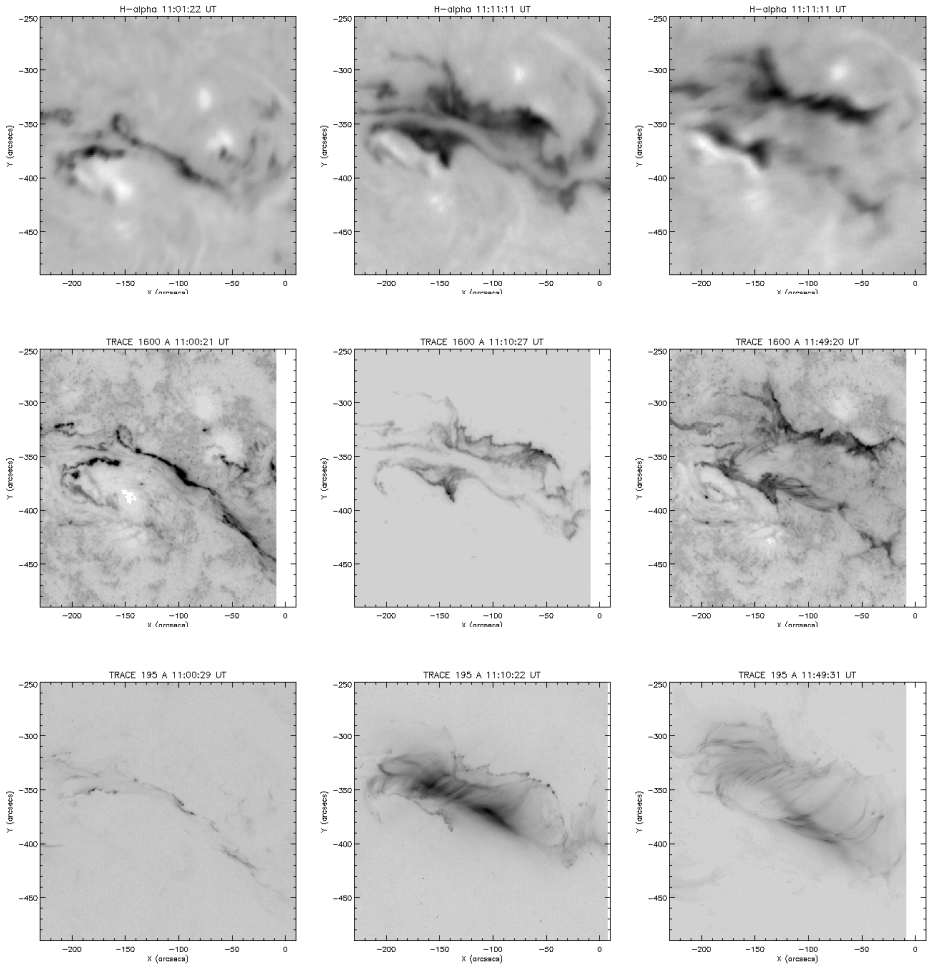

Figure 4. Hα, TRACE 1600 Å and 195 Å negative images of the 4B/X17.2 flare at begin, max and in decay phase. North is up and west is to the right.

3.3 *Active region complexity*

On 28 October 2003, NOAA AR 10486 was located at S16 E08 and passed over the solar disk from 23 October to 4 November 2003. The active region has $\beta\gamma\delta$ magnetic configuration. It was the largest and most complex active region of current solar cycle 23. During its passage on solar disk it produces 7 X class, 15 M class and many small solar flares. In the active region a thin corridor of negative polarity flux bisects the strong positive polarity area in the central part of the active region. The presence of sigmoid filaments in the active region shows a highly sheared magnetic field in which a large amount of free magnetic energy gets stored (Singh & Gupta 1995; Uddin & Verma 1998; Schmieder *et al.* 1993). Zhang *et al.* (2003) also reported the high shear $\sim 90^{\circ}$ in this active region. From the SOHO/MDI magnetogram movie we noticed the fast emergence and cancellation of magnetic flux in the active region.

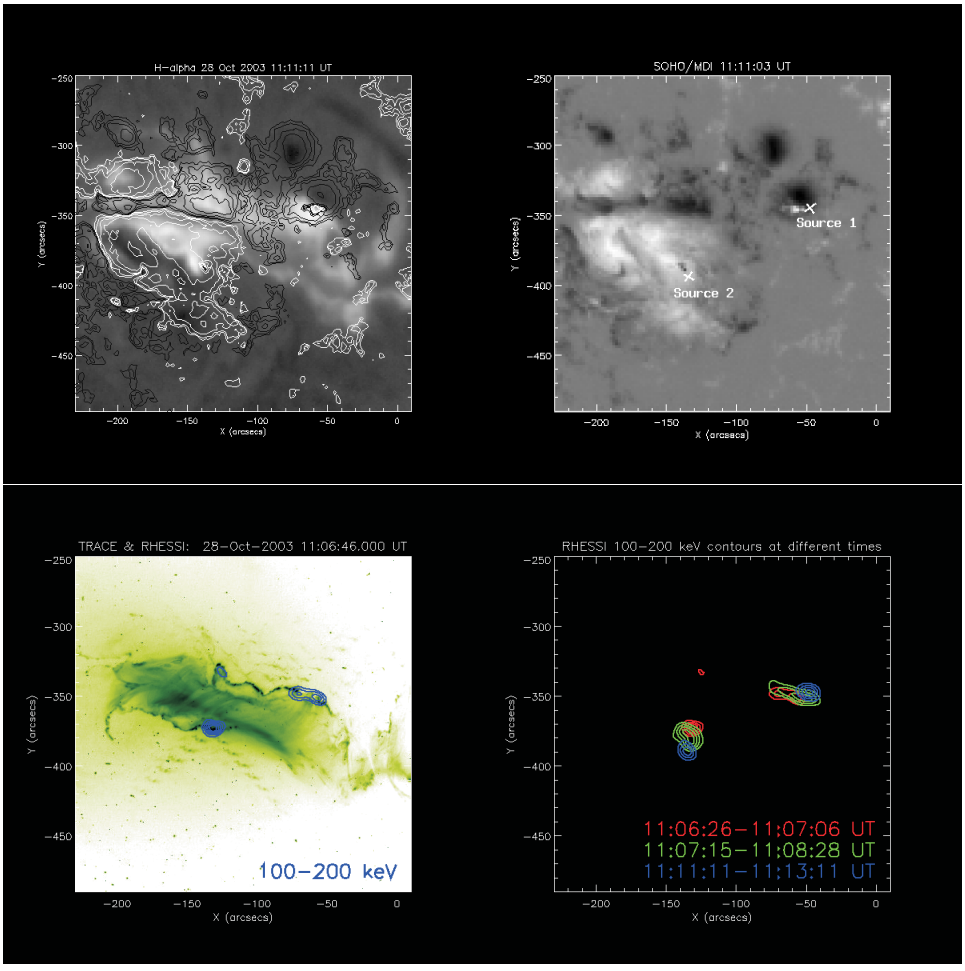

Figure 5. Hα image of the flare overlaid by MDI contours (level = $\pm$100, $\pm$200, $\pm$400, $\pm$800, $\pm$1600 gauss), MDI magnetogram overlaid by location of RHESSI HXR source (circle symbol), TRACE 195 Å image overlaid by RHESSI source and location of RHESSI HXR sources at three selected times. North is up and west is to the right.

3.4 *Energetics of the filament, flare and CME*

The disappearance of the sigmoid filaments is an indicator of a large scale change of coronal magnetic field (Tang *et al.* 1999). Dynamic filament eruption are generally associated with energetic solar flares, CMEs, etc. Therefore the energy stored in filament plays an important role in the production of these energetic phenomena.

Taking this into account we tried to estimate the energy stored in the filaments F1, F2 and F3, which erupted producing 4B/X17.2 superflare and high speed halo CME. The eruption of three major filaments was associated with this superflare and associated phenomena. So to understand the energetics of these filaments and its association with flare and CME energetics we estimated the total energy stored in all three filaments using the circuit model of Martens *et al.* (1986) and Martens & Quin (1989). The

parameter for the energy calculation is derived using our Hα data. The estimated values of the energy stored in these three active region sigmoid filaments are 5.26×10^{34}, 1.20×10^{34} and 1.71×10^{34} ergs respectively and the total energy stored in all three filaments is 8.16×10^{34} ergs.

Following White *et al.* (2005) we measure the temperature and emission measure during flare maximum phase using the GOES data and the values are 22.24 MK and 42.14×10^{49} cm^{-3} respectively. Using these temperature and emission measure values we calculate the thermal energy ($E_{\rm th}$) content of the flare applying the following formula:

$$E_{\rm th} = 3\,{\rm kT}\sqrt{EM \cdot V},$$

where k, T, EM and V are the Boltzmann constant, temperature, emission measure and volume of the source respectively. The volume of the source is calculated using the RHESSI 10–20 keV images taking the 45% of contour level. The calculated value of the thermal energy content in the flare is 1.9×10^{31} ergs.

Magnetic reconnection is the main possible cause for the energy release process in solar flares. The reconnection rate is one of the most important parameters in this process. The reconnection rate can be calculated using the formula $\dot{\Phi} = B_c v_i$ (Asai *et al.* 2002), where B_c and v_i are the coronal magnetic field and inflow velocity into the reconnection region respectively. Assuming the magnetic field is conserved then the reconnection rate can be expressed as $\dot{\Phi} = B_p v_f$, where B_p is the photospheric magnetic field and v_f is the ribbon separation speed respectively. For this flare we calculated the value of the reconnection rate at three HXR sources which are spatially correlated with Hα kernels viz., K1, K2 and K3. The calculated values of the reconnection rate at kernels K1, K2 and K are 70 volt cm^{-1}, 56 volt cm^{-1} and 35 volt cm^{-1} respectively.

The mass, projected velocity and kinetic energy of the CME associated with this flare have been given in SOHO LASCO catalog (http://cdaw.gsfc.nasa.gov/CME_list/UNIVERSAL/text_ver/). The values of the mass, projected velocity and the kinetic energy of the CME are 4.0×10^{16} gm, 2459 km s^{-1}, 1.2×10^{33} erg respectively. We compared the value of kinetic energy and the value of the thermal energy content of the flare and found that the thermal energy content of the flare is 2 orders smaller than the kinetic energy of the CME.

3.5 *Coronal mass ejections and other associated phenomena*

A full halo CME with very bright emittance all around the occulting disc of the SOHO/LASCO coronagraph was associated with this flare. The event was first observed on C2 at 10:54 UT as a bright loop front over the West limb, by 11:30 UT the front had developed into a full halo CME. The front first appeared as a full halo CME in C3 at 11:42 UT. In the EUV region, according to SOHO/EIT data, it was accompanied by a coronal wave propagating in the northern hemisphere and dimmings extended over all the southern hemisphere. The CME was very fast and the speed was 2458 km s^{-1}. Comparing the direction of filaments (F1 and F3) eruption and the CME direction indicates that the CME was associated with the eruption of these filaments.

The flare was associated with several different types of radio bursts. The radio bursts consist of a group of rapidly drifting type III bursts and a complicated system of more

slowly drifting diffuse type II (speed 1250 km s^{-1}) with fundamental-harmonic structure followed by a type IV continuum. This flare has intense radio bursts including a 245 MHz burst near 500,000 sfu, a Tenflare of 13,000 sfu. The space weather disturbances associated with this flare are characterized by an extremely strong increase in the high-energy proton flux (29,500 pfu $>$ 10 MeV) and a severe geomagnetic storm with D_{st} index -363 nT. This flare is a strong cosmic ray event and produces unusual Ground Level Enhancement (GLE). Bieber *et al.* (2005) analyzed and described many unusual features of the GLE associated with this flare.

4. Discussion and conclusions

The 4B/X17.2 flare observed at ARIES in Hα was associated with filament eruptions, fast full halo CME, different types of strong radio bursts, strong proton flare, etc.

The flare shows the multi-ribbon structure. The flare has two main parallel ribbons in the opposite magnetic polarity regions. From the comparison of Hα flare in UV and EUV wavebands we conclude that the flare shows a similar type of morphology in Hα, EUV and UV wavelengths.

We measure the value of the magnetic field at three HXR sources and find that it corresponds to high magnetic field strength. Normally the HXR sources are found to be associated with weak magnetic field regions. However, Asai *et al.* (2002) found the HXR sources to be associated with high magnetic field regions. So our results confirm the finding of Asai *et al.* (2002).

We derived the magnetic reconnection rate at the HXR sources measuring the Hα ribbon motions and photospheric magnetic field at HXR sources. We found that reconnection rate at kernels K1, K2 and K3 are 70 volt cm^{-1}, 56 volt cm^{-1} and 35 volt cm^{-1} respectively. The values are one order greater than the reported value of Poletto and Kopp (1986) and comparable with the values of Qiu *et al.* (2002). Such large values of magnetic reconnection rate may be due to the fact that the flare kernels are moving towards the sunspots and cover the sunspot umbrae, where the magnetic field is very strong.

We compared the kinetic energy of the CME, thermal energy content of the flare and stored energy in the twisted sigmoid filaments (F1, F2 and F3). The thermal energy content of the flare was found to be 2nd order of magnitude less than the CME kinetic energy. Recently Emsile *et al.* (2004) analyzed two events, and found that the CME kinetic energy was found to be almost 1 order larger than the flare energy. We also compared the energy stored in sigmoid filaments, flare thermal energy and the kinetic energy of the CME and found that the energy stored in the sigmoid filament is 1 order higher than CME energy, however 3 orders higher than the thermal energy content of the flare. Hence we conclude that the filaments F1, F2 and F3 have more than sufficient energy to trigger the flare, CME and other energetic phenomena.

References

Asai *et al.* 2002, *ApJ*, **586**, 624.
Bieber, W. J. *et al.* 2005, *Geophys. Res. Lett.*, **32**, L03S02, doi:10.1029/2004/GR:0214892.
Bougeret, J.-L. *et al.* 1995, *Space Sci. Rev.*, **71**, 231.
Brueckner, J.-L. *et al.* 1995, *Solar Phys.*, **162**, 357.
Delaboudiniere, J.-P. *et al.* 1995, *Solar Phys.*, **162**, 357.

Donea, A.-C., Lindsey, C. 2005, *ApJ*, **630**, 1168.
Emslie, A. G. *et al.* 2004, *J. Geophys. Res. A.*, **109**, 10104.
Gopalswamy, N. *et al.* 2005, *J. Geophys. Res. A.*, **110**, A09S00, doi: 10.1029/2005JA011268.
Grechnev, V. V *et al.* 2005, *J. Geophys. Res. A.*, **110**, A09S07, doi: 10.1029/2004JA010931.
Handy, B. N. *et al.* 1999, *Solar Phys.*, **187**, 229.
Krucker, S., Hudson, H. S. 2004, *Proc. of the SOHO 15 Workshop- Coronal heating, St. Andrews, Scotland, 6–9 September 2004 (ESA SP - 575, December 2004), p. 247.*
Klassen, A. *et al.* 2005, *J. Geophys. Res. A.*, **110**, A09S04, doi:10.1029/2004JA010910.
Lin, R. P. *et al.* 2002, *Solar Phys.*, **210**, 3.
Luthi, T., Ludi, A., Magun, A. N. 2004, *Astron. Astrophys.*, **420**, 361.
Martens, P. C. H. *et al.* 1986, *Solar Phys.*, **107**, 95.
Martens, P. C. H., Kuin, N. P. M. 1989, *Solar Phys.*, **22**, 263.
Pick, M., Jean-Marie, K. A., Maia, D. J. F. 2005, *ApJL*, **661**, 97.
Poletto, G., Kopp, R. A. 1986, In: The lower atmosphere of solar flares (ed.) Neidig, D. F. (Sunspot: NSO), 453.
Qiu, J., Lee, J., Gray, D. E., Wang, H. 2002, *ApJ*, **565**, 1355.
Schmieder, *et al.* 1993, *Adv. Space Res.*, **13**, 119.
Singh, J, Gupta, S. S. 1995, *Solar Phys.*, **158**, 259.
Scherrer, P. H. *et al.* 1995, *Solar Phys.*, **162**, 129.
Tang *et al.* 1999, *Solar Phys.*, **185**, 143.
Uddin, W., Verma, V. K. 1998, *BASI*, **26**, 317.
White, S. M., Thomas, R. J., Schwartz, R. A. 2005, *Solar Phys.*, **227**, 231.
Zhang, Hong-Qi *et al.* 2003, *Chinese J. Astron. Astrophys.*, **3**, 491.